Advanced Composite Materials
Publication details, including instructions for authors and subscription information:
http://www.tandfonline.com/loi/tacm20

Numerical modeling of the effective electromechanical properties of cellular piezoelectret film by asymptotic homogenization

Yongping Wan [a], Liangliang Fan [a] & Haibing Yu [a]
[a] School of Aerospace Engineering and Applied Mechanics, Tongji University, Shanghai, 200092, P.R. China
Published online: 18 Mar 2013.

To cite this article: Yongping Wan, Liangliang Fan & Haibing Yu (2013) Numerical modeling of the effective electromechanical properties of cellular piezoelectret film by asymptotic homogenization, Advanced Composite Materials, 22:2, 123-138, DOI: 10.1080/09243046.2013.780281

To link to this article: http://dx.doi.org/10.1080/09243046.2013.780281

Advanced Composite Materials, 2013
Vol. 22, No. 2, 123–138, http://dx.doi.org/10.1080/09243046.2013.780281

Numerical modeling of the effective electromechanical properties of cellular piezoelectret film by asymptotic homogenization

Yongping Wan*, Liangliang Fan and Haibing Yu

School of Aerospace Engineering and Applied Mechanics, Tongji University, Shanghai 200092, P.R. China

(*Received 22 October 2012; accepted 22 February 2013*)

Cellular piezoelectret film is actually the voided charged polymer foam that, macroscopically, shows significant quasi-piezoelectricity in the thickness direction. In this study, cellular piezoelectret film is viewed as a periodic composite, where the charged microvoids are taken as piezoelectric inclusions scattered periodically in the host polymer matrix. Based on the asymptotic homogenization for piezoelectric composite implemented by finite element method, the effective electromechanical properties of cellular piezoelectret film are numerically modeled. Dependence of the overall electromechanical properties on various material parameters and geometric variables of voids is explored. The inflation experiments of cellular piezoelectret film published in the literature can also be numerically simulated. It is shown that the overall properties of cellular piezoelectret film can be effectively simulated by the asymptotic homogenization based on finite element analysis. This approach can be an efficient mean for the numerical simulation of the overall properties in the optimization design of cellular piezoelectret film with complex microvoid structures.

Keywords: cellular piezoelectret film; periodic composite; overall electromechanical properties; asymptotic homogenization; finite element analysis

1. Introduction

There has been a resurgence of interests in the effort to develop new piezoelectric materials. Cellular piezoelectret film is a new member of the functional materials that show remarkable quasi-piezoelectric effect.[1] Cellular piezoelectret film is actually voided charged polymer foam. It is generally prepared from polymer, such as polypropylene (PP), by means of biaxial stretching and electric charging. The action of biaxial stretching on a polymer premixed with fine mineral particles leads to many lens-like microvoids scattered. Corona charging process is usually taken to the voided polymer film. Charges of opposite polarities are trapped and reside separately on the top and bottom part of the void internal surface.[2] Upon external mechanical pressure, the voided charged polymer film can be piezoelectric and is, therefore, called cellular piezoelectret. The quasi-piezoelectricity in the film thickness direction can be comparable with that of the traditional piezoelectric ceramics.[3] In addition, the film also has the advantage of lightweight, flexibility, easiness to fabricating, no poison pollution, cost-effectiveness as well as the low impedance matching water and human body. All these advantages make this material very attractive in the flexible electromechanical sensors and

*Corresponding author. Email: wanyp@tongji.edu.cn

transducers. Cellular piezoelectret film now shows great potential in the electro-acoustic application, such as in the area of medical diagnostics, surveillance and nondestructive testing in biological technology, etc.[4]

Understanding of material preparation has been advanced significantly so far.[5] Some technologies have been proposed to improve the quasi-piezoelectric coefficient. For example, the piezoelectric activity of cellular piezoelectret PP films can be remarkably increased by thickness expansion.[6,7] The improvement of d_{33} coefficient is due to the decrease in Young's modulus in the film thickness direction as well as the increase in chargeability owing to expansion. At the same time, research on improvement in thermal stability has also been carried out. Cellular piezoelectret with polytetrafluoroethylene and tetrafluoroethylene–hexafluoropropylene copolymer as the host polymer, for example, exhibits a greater stability for the piezoelectric activity at 90 °C, compared with the traditional PP piezoelectrets.[8]

On the aspect of theoretical model, Paajanen et al. [9,10] simplified the layered piezoelectret as the one air gap structure. Elementary models were developed to evaluate the sensitivity for the actuator and sensor mode. In terms of the theoretical model, Young's moduli of the films can be determined using data from sensor and actuator sensitivity measurements. Sessler and Hillenbrand [11] and Hillenbrand et al. [12] developed the sandwich model of alternating parallel plane polymer layers and air layers. Qualitative analysis was provided to confirm experimental observation that d_{33} is inversely proportional to the overall modulus in the thickness direction.[11,12] A more sophisticated model [13] was developed using the coupled mean field micro-electromechanical model to predict the macroscopic piezoelectric behavior. The differential effective medium model was adopted in approximating the effective stiffness, dielectric permittivity, and piezoelectric coupling coefficients. This approach improves the approximation of piezoelectret behavior by capturing the influence of microscopic material structure on macroscopic piezoelectric performance. Wan et al. [14] developed a micromechanical model using the Eshelby equivalent inclusion method to find the effective electromechanical properties of cellular piezoelectret polymer foam. In this formulation, the voids with surplus charge are deemed as ellipsoidal heterogeneous inclusions which show piezoelectric-like effect under deformation and the matrix is the nonpolar polymer. In addition to the qualitative discussion on the sensitivity of electromechanical properties with respect to various parameters, quantitative comparison with experiment data was also presented. Furthermore, the authors extended this micromechanical model to viscoelastic matrix to predict the time-dependent behavior of the overall piezoelectric d_{33} coefficient of voided charged polymer foam.[15,16]

With regard to numerical simulation of piezoelectret, Tuncer et al. [17] conducted a finite element analysis on the two- and three-layer piezoelectret systems by using Femlab. The simulation takes into account the coupling of electrical and mechanical stresses in terms of the Maxwell stress tensor. Focusing on the cellular piezoelectret films with complex microstructures where analytical solution is generally unavailable, Wan and Fan [18] modeled the flat voids by the hollow oblate tetrakaidecahedron scattered periodically in the host polymer. Charges of opposite polarities are assumed to be distributed on the upper and lower part of the internal surfaces. The electrostatic field and the deformation are numerically solved. The piezoelectric d_{33} coefficient is defined and obtained in terms of the inverse piezoelectric effect. Furthermore, by considering the viscoelastic property of the host polymer, they [19] also extend this finite element method (FEM) to simulate the temporal evolution of the effective piezoelectric d_{33} coefficient.

As is known, the quasi-piezoelectric effect of voided charged polymer film is intimately connected with shape anisotropy of microvoids. Design of cellular piezoelectret polymer film with more advanced properties generally needs the topology optimization of the internal void

structures. Powerful analysis tool, such as FEM, is necessary in the optimization design of cellular piezoelectret films with complex void microstructures. However, since the microvoids are generally very small compared with the ordinary devices made of cellular piezoelectret materials, analysis of piezoelectret devices directly using FEM on the microscale level usually results in huge computer calculation work and sometimes becomes intractable. Asymptotic homogenization has long been developed to treat the effective properties of composite with large amount of inhomogeneities.[20] For periodic piezoelectric composites where the electroelastic coupling equation with rapidly oscillating coefficients can be established, the asymptotic homogenization plus FEM [21–23] has been adopted to find the effective properties. In this study, the effective electromechanical properties of cellular piezoelectret film are analyzed by means of the asymptotic homogenization implemented by FEM. Cellular piezoelectret film is taken as periodic composite. The flat microvoids are modeled by the hollow oblate tetrakaidecahedron.[18,19] The smallest repetitive cuboid that compactly encloses the tetrakaidecahedron actually serves as the unit cell. The dependence of the overall electromechanical properties on various material parameters and geometric variables of voids are explored. The results of inflation experiment of cellular piezoelectret film published in the literature have been numerically reproduced. It is shown that the overall properties of cellular piezoelectret film can be effectively simulated by the approach of asymptotic homogenization plus finite element.

2. Asymptotic homogenization implemented by FEM

The homogenization method has been extensively studied during the past several decades for periodic composite in the quasi-static application where wavelength is much larger than the microstructures. Here, we briefly present the theory of asymptotic homogenization applied to piezoelectricity, with the emphasis on the finite element implementation for the effective electromechanical coefficients of cellular piezoelectret polymer composite.

2.1. Theory of asymptotic homogenization for piezoelectricity

In a piezoelectric material, the electromechanical fields can be described by the piezoelectric equations as,

$$\sigma_{ij} = c_{ijkl}u_{k,l} + e_{kij}\varphi_{,k} \tag{1}$$

$$D_i = e_{ikl}u_{k,l} - k_{ik}\varphi_{,k} \tag{2}$$

where c_{ijkl}, e_{kij}, and k_{ik} are the elastic modulus, piezoelectric coefficient and the dielectric permittivity. σ_{ij} and D_k are the elastic stress and the electric displacements. u_i and φ are the mechanical displacements and electric potential, which, in the case of piezoelectric composite with large amount of inhomogeneities, can be asymptotically expanded as

$$u_i = u_i^0(x_j) + \delta u_i^1(x_j, y_j) + \delta^2 u_i^2(x_j, y_j) + \ldots\ldots \tag{3}$$

$$\varphi = \varphi^0(x_j) + \delta\varphi^1(x_j, y_j) + \delta^2\varphi^2(x_j, y_j) + \ldots\ldots \tag{4}$$

where x_i denote the global coordinate. y_i the local coordinate that is defined in the smallest repeated unit cell, that is, the representative volume element (RVE). They are mutually related

by $y_i = x_i/\delta$, where δ is a small parameter. u_i^0 and φ^0 are macroscopic displacement and electric potential, while $u_i^1, u_i^2 \ldots$ and $\varphi^1, \varphi^2 \ldots$ are periodic function with respect to the local coordinate y_i. Usually, only the first terms, that is, u_i^1 and φ^1, are retained in the expansion, which represent the displacement and electric potential on the microscopic level. The macroscopic and microscopic fields are related by

$$u_i^1(x,y) = \chi_i^{kl}(y)e_{xkl}(u_i^0) + \Pi_i^j(y)\phi_{xj}(\varphi^0) \tag{5}$$

$$\varphi^1(x,y) = \Gamma^{kl}(y)e_{xkl}(u_i^0) + \Lambda^j(y)\phi_{xj}(\varphi^0) \tag{6}$$

where $\chi_i^{kl}(y)$ are the characteristic displacements and $\Lambda^j(y)$ is the characteristic electrical potential of the unit cell. $\Pi_i^j(y)$ and $\Gamma^{kl}(y)$ are the characteristic coupled functions.[21]

$$e_{xkl}(u_i^0) = \frac{1}{2}\left(\frac{\partial u_k^0}{\partial x_l} + \frac{\partial u_l^0}{\partial x_k}\right) \tag{7}$$

$$\phi_{xi}(\varphi^0) = -\frac{\partial \varphi^0}{\partial x_i} \tag{8}$$

The characteristic terms should be obtained by solving the local problems, which are defined on the RVE, and governed by the following equations [21]:

$$\frac{\partial}{\partial y_j}\left[c_{ijkl}(T_{mh}^{kl} + e_{ykl}(\chi_i^{mh})) + e_{kij}\frac{\partial \Gamma^{mh}}{\partial y_k}\right] = 0 \tag{9}$$

$$\frac{\partial}{\partial y_i}\left[e_{ikl}(T_{mh}^{kl} + e_{ykl}(\chi_i^{mh})) - k_{ik}\frac{\partial \Gamma^{mh}}{\partial y_k}\right] = 0 \tag{10}$$

$$\frac{\partial}{\partial y_j}\left[c_{ijkl}e_{ykl}(\Pi_i^n) - e_{kij}\left(\delta_{kn} - \frac{\partial \Lambda^n}{\partial y_k}\right)\right] = 0 \tag{11}$$

$$\frac{\partial}{\partial y_i}\left[e_{ikl}e_{ykl}(\Pi_i^n) + k_{ik}\left(\delta_{kn} - \frac{\partial \Lambda^n}{\partial y_k}\right)\right] = 0 \tag{12}$$

In the above equations, there are

$$e_{ykl}(\chi_i^{mh}) = \frac{1}{2}\left(\frac{\partial \chi_k^{mh}}{\partial x_l} + \frac{\partial \chi_l^{mh}}{\partial x_k}\right), e_{ykl}(\Pi_i^n) = \frac{1}{2}\left(\frac{\partial \Pi_k^n}{\partial y_l} + \frac{\partial \Pi_l^n}{\partial y_k}\right) \tag{13a,b}$$

The symbol '∂' represents partial differentiation. T_{mh}^{kl} is the fourth order unit tensor,

$$T_{mh}^{kl} = \frac{1}{2}(\delta_{km}\delta_{lh} + \delta_{kh}\delta_{lm}) \tag{14}$$

where δ_{ij} is the Kronecker delta. Once the characteristic terms in Equations (5) and (6) are solved, the homogenized coefficients can be found by Ref. [21],

$$\bar{c}_{ijmh} = \frac{1}{V}\int_Y \left[c_{ijkl}\left(T^{kl}_{mh} + \frac{\partial \chi^{mh}_k}{\partial y_l} \right) + e_{kij}\frac{\partial \Gamma^{mh}}{\partial y_k} \right] dY \tag{15}$$

$$\bar{e}_{imh} = \frac{1}{V}\int_Y \left[e_{ikl}\left(T^{kl}_{mh} + \frac{\partial \chi^{mh}_k}{\partial y_l} \right) - k_{ik}\frac{\partial \Gamma^{mh}}{\partial y_k} \right] dY \tag{16}$$

$$\bar{k}_{in} = \frac{1}{V}\int_Y \left[e_{ikl}\frac{\partial \Pi^n_k}{\partial y_l} + k_{ik}\left(\delta_{kn} - \frac{\partial \Lambda^n}{\partial y_k} \right) \right] dY \tag{17}$$

where the quantities with an over bar represent the homogenized properties, V is the volume of the RVE.

2.2. *Geometric model and finite element formulation*

Since the microvoids are produced by the biaxial stretching on a polymer premixed with fine mineral particles, which can be assumed to be homogeneously scattered, cellular piezoelectret film (Figure 1) can be considered as the periodic composite where the closed flat voids are aligned periodically in polymer matrix, as was done in previous theoretical treatment.[14–16] Electric charges are usually assumed to be distributed uniformly on the internal surfaces of microvoids. The charged voids behave piezoelectric-like under mechanical deformation and can be regarded as piezoelectric inclusions. With suitable definition, piezoelectric coefficients can be defined.[14–16] The microvoid can be geometrically modeled by the hollow oblate tetrakaidecahedron.[18,19] It can be verified that the space can be seamlessly filled when the hollow oblate tetrakaidecahedra are periodically arranged, as shown in Figure 2. The RVE is selected to be the cuboid which compactly enclose the hollow oblate tetrakaidecahedron, [18,19] as shown in Figure 3. The in-plane sizes, that is, the lengths in the two orthogonal directions in the $y_1 - y_2$ plane, are identical and denoted by a, while the height in y_3 direction is given by h. The hollow oblate tetrakaidecahedron has the wall thickness of t. The aspect ratio can be defined as [18,19]

$$k = (h - 2t)/(a - 2t) \tag{18}$$

and the void volume fraction is,

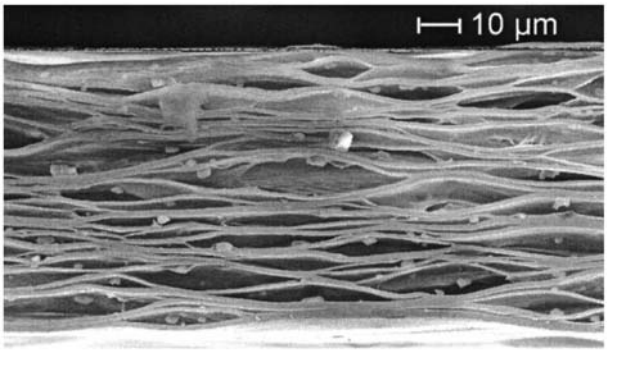

Figure 1. Cellular PP film.

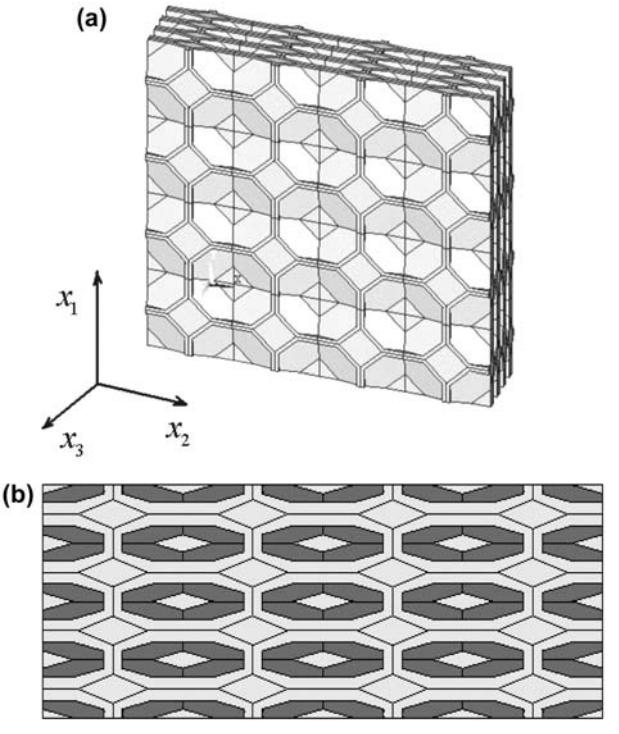

Figure 2. (a) Periodic composite and (b) sectional view.

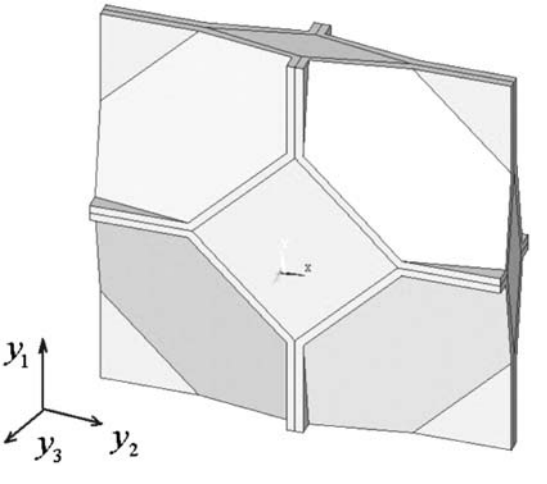

Figure 3. The RVE.

$$f = (h - 2t)(a - 2t)^2/(a^2 h) \tag{19}$$

The asymptotic homogenization method (AHM) is based on rigorous mathematical deduction. The calculated effective properties of periodic composite depend on the results of a local analysis on the RVE, which is usually carried out by FEM. Therefore, this analysis procedure

is known as AHM plus FEM.[20–23] In this study, the local analysis is carried out in ANSYS. The SOLID5 element, which is 8-node hexahedron isoparametric coupling element, is used here to mesh the RVE. The discrete formulation of finite element is as follows,

$$\int_Y \mathbf{B}^T\mathbf{D}\mathbf{B}dY\begin{bmatrix}\boldsymbol{\chi}^{mh}\\ \boldsymbol{\Gamma}^{mh}\end{bmatrix} = -\int_Y \mathbf{B}^T\mathbf{D}\boldsymbol{\varepsilon}_0^{mh}dY \tag{20a}$$

$$\int_Y \mathbf{B}^T\mathbf{D}\mathbf{B}dY\begin{bmatrix}\boldsymbol{\Pi}^{n}\\ \boldsymbol{\Lambda}^{n}\end{bmatrix} = -\int_Y \mathbf{B}^T\mathbf{D}\mathbf{E}_0^{n}dY \tag{20b}$$

where

$$\begin{bmatrix}\boldsymbol{\chi}^{mh}\\ \boldsymbol{\Gamma}^{mh}\end{bmatrix} = \left[\begin{pmatrix}\chi_1^{mh}\\ \Gamma_1^{mh}\end{pmatrix}^T\begin{pmatrix}\chi_2^{mh}\\ \Gamma_2^{mh}\end{pmatrix}^T\begin{pmatrix}\chi_3^{mh}\\ \Gamma_3^{mh}\end{pmatrix}^T\begin{pmatrix}\chi_4^{mh}\\ \Gamma_4^{mh}\end{pmatrix}^T\begin{pmatrix}\chi_5^{mh}\\ \Gamma_5^{mh}\end{pmatrix}^T\begin{pmatrix}\chi_6^{mh}\\ \Gamma_6^{mh}\end{pmatrix}^T\begin{pmatrix}\chi_7^{mh}\\ \Gamma_7^{mh}\end{pmatrix}^T\begin{pmatrix}\chi_8^{mh}\\ \Gamma_8^{mh}\end{pmatrix}^T\right]^T \tag{21a}$$

$$\begin{bmatrix}\boldsymbol{\Pi}^{n}\\ \boldsymbol{\Lambda}^{n}\end{bmatrix} = \left[\begin{pmatrix}\Pi_1^{n}\\ \Lambda_1^{n}\end{pmatrix}^T\begin{pmatrix}\Pi_2^{n}\\ \Lambda_2^{n}\end{pmatrix}^T\begin{pmatrix}\Pi_3^{n}\\ \Lambda_3^{n}\end{pmatrix}^T\begin{pmatrix}\Pi_4^{n}\\ \Lambda_4^{n}\end{pmatrix}^T\begin{pmatrix}\Pi_5^{n}\\ \Lambda_5^{n}\end{pmatrix}^T\begin{pmatrix}\Pi_6^{n}\\ \Lambda_6^{n}\end{pmatrix}^T\begin{pmatrix}\Pi_7^{n}\\ \Lambda_7^{n}\end{pmatrix}^T\begin{pmatrix}\Pi_8^{n}\\ \Lambda_8^{n}\end{pmatrix}^T\right]^T \tag{21b}$$

$$\mathbf{B} = \left[\mathbf{B}_1^e\ \mathbf{B}_2^e\ \mathbf{B}_3^e\mathbf{B}_4^e\ \mathbf{B}_5^e\ \mathbf{B}_6^e\ \mathbf{B}_7^e\ \mathbf{B}_8^e\right] \tag{22}$$

$$\mathbf{B}_i^e = \begin{bmatrix}\partial N_i^e/\partial y_1 & 0 & 0 & 0\\ 0 & \partial N_i^e/\partial y_2 & 0 & 0\\ 0 & 0 & \partial N_i^e/\partial y_3 & 0\\ 0 & \partial N_i^e/\partial y_3 & \partial N_i^e/\partial y_2 & 0\\ \partial N_i^e/\partial y_3 & 0 & \partial N_i^e/\partial y_1 & 0\\ \partial N_i^e/\partial y_2 & \partial N_i^e/\partial y_1 & 0 & 0\\ 0 & 0 & 0 & -\partial N_i^e/\partial y_1\\ 0 & 0 & 0 & -\partial N_i^e/\partial y_2\\ 0 & 0 & 0 & -\partial N_i^e/\partial y_3\end{bmatrix} \tag{23}$$

$$\boldsymbol{\chi}_i^{mh} = \begin{Bmatrix}\chi_{1i}^{mh}\\ \chi_{2i}^{mh}\\ \chi_{3i}^{mh}\end{Bmatrix},\ \boldsymbol{\Pi}_i^{n} = \begin{Bmatrix}\Pi_{1i}^{n}\\ \Pi_{2i}^{n}\\ \Pi_{3i}^{n}\end{Bmatrix} \tag{24a, b}$$

in which, $i = 1, 2, \ldots, 8$ are the node number,

$$\mathbf{D} = \begin{bmatrix}\mathbf{C} & -\mathbf{e}^T\\ \mathbf{e} & \mathbf{k}\end{bmatrix} \tag{25}$$

C, **e**, and **k** are, respectively, the elastic stiff matrix, the piezoelectric stress coefficient matrix, and the dielectric matrix. The superscript 'T' refers to matrix transpose. $\boldsymbol{\varepsilon}_0^{mh}$ the unit initial strain vector, and $\mathbf{E}_0^n$ the unit initial electric field vector, where the superscript indices, that is, m, h, and n, value range from 1 to 3. The right-hand side of the Equations (20a) and (20b)

can be understood as the node force induced, respectively, by the unit initial strain exerted on the '*mh*' direction or the unit initial electric field exerted in the 'n' direction. After solving Equations (20a) and (20b), $\boldsymbol{\chi}^{mh}$, $\boldsymbol{\Gamma}^{mh}$, $\boldsymbol{\Pi}^{n}$, and $\boldsymbol{\Lambda}^{n}$ can be obtained, which can further be inserted into Equations (15)–(17) to find the effective elastic matrix, the effective piezoelectric coefficient and also the effective dielectric matrix. Generally, there are six different loads in Equations (20a) as '*mh*' in turn takes the value of 11, 22, 33, and 12 or 21, 23 or 32, 13 or 31, respectively. Also in Equations (20b), there are three different loads, when '*n*' equals to 1–3. Therefore, there usually total nine cases of loads in order to completely determine the effective properties.

2.3. Implementation of finite element (FE) method and the effective elastic and piezoelectric properties

Due to the isotropy of host polymer and the structure symmetry of the oblate spherical microvoids, we can judge that the effective property of cellular piezoelectret film is transversely isotropic, as demonstrated in experiments.[2–4] The overall piezoelectric strain coefficients matrix $[\bar{d}]$ can be found by,

$$[\bar{d}] = [\bar{e}][\bar{S}] \tag{26}$$

where $[\bar{e}]$ is the piezoelectric stress coefficient matrix, $[\bar{S}]$ the elastic compliance matrix which is inverse to the elastic stiffness, $[\bar{C}]$. For cellular piezoelectret film, the concerned parameters are usually the overall $\bar{d}_{33}$ and $\bar{d}_{31} = \bar{d}_{32}$, which, in terms of Equation (26), can be given by,

$$\bar{d}_{31} = \bar{S}_{11}\bar{e}_{31} + \bar{S}_{12}\bar{e}_{32} + \bar{S}_{13}\bar{e}_{33} \tag{27a}$$

$$\bar{d}_{32} = \bar{S}_{12}\bar{e}_{31} + \bar{S}_{22}\bar{e}_{32} + \bar{S}_{23}\bar{e}_{33} \tag{27b}$$

$$\bar{d}_{33} = \bar{S}_{13}\bar{e}_{31} + \bar{S}_{23}\bar{e}_{32} + \bar{S}_{33}\bar{e}_{33} \tag{27c}$$

In order to find the piezoelectric strain coefficients $\bar{d}_{31}$ (or $\bar{d}_{32}$) and $\bar{d}_{33}$, the overall elastic compliance, $\bar{S}_{11} = \bar{S}_{22}$, $\bar{S}_{12}$, $\bar{S}_{13} = \bar{S}_{23}$, $\bar{S}_{33}$, and the overall piezoelectric stress coefficients, $\bar{e}_{33}$, $\bar{e}_{31} = \bar{e}_{32}$, should be predetermined. The above-mentioned elastic compliance can be found once the overall elastic stiff coefficients, that is, $\bar{C}_{11} = \bar{C}_{22}$, $\bar{C}_{12}$, $\bar{C}_{13} = \bar{C}_{23}$, $\bar{C}_{33}$, are solved. This can be accomplished by the analysis of the local problem dictated by Equations (20a) and (20b) with only two cases of loads, that is, $m = h = 3$ and $m = h = 1$. For the load case of $m = h = 3$, a unit initial strain is applied in the y_3 direction, that is,

$$\boldsymbol{\varepsilon}_0^{33} = [\,0 \quad 0 \quad 1 \quad 0 \quad 0 \quad 0 \quad 0 \quad 0 \quad 0\,]^T \tag{28}$$

Then, in terms of Equations (15) and (16), the following effective properties can be obtained,

$$\bar{C}_{33} = \frac{1}{V}\int_Y \left(C_{33} + C_{31}\frac{\partial \chi_1^{33}}{\partial y_1} + C_{32}\frac{\partial \chi_2^{33}}{\partial y_2} + C_{33}\frac{\partial \chi_3^{33}}{\partial y_3} + e_{33}\frac{\partial \Gamma^{33}}{\partial y_3} \right) dY \tag{29a}$$

$$\bar{C}_{13} = \frac{1}{V}\int_Y \left(C_{13} + C_{11}\frac{\partial \chi_1^{33}}{\partial y_1} + C_{12}\frac{\partial \chi_2^{33}}{\partial y_2} + C_{13}\frac{\partial \chi_3^{33}}{\partial y_3} + e_{31}\frac{\partial \Gamma^{33}}{\partial y_3} \right) dY \tag{29b}$$

$$\bar{C}_{23} = \frac{1}{V}\int_Y \left(C_{23} + C_{21}\frac{\partial \chi_1^{33}}{\partial y_1} + C_{22}\frac{\partial \chi_2^{33}}{\partial y_2} + C_{23}\frac{\partial \chi_3^{33}}{\partial y_3} + e_{32}\frac{\partial \Gamma^{33}}{\partial y_3} \right) dY \tag{29c}$$

$$\bar{e}_{33} = \frac{1}{V}\int_Y \left(e_{33} + e_{31}\frac{\partial \chi_1^{33}}{\partial y_1} + e_{32}\frac{\partial \chi_2^{33}}{\partial y_2} + e_{33}\frac{\partial \chi_3^{33}}{\partial y_3} - k_{33}\frac{\partial \Gamma^{33}}{\partial y_3} \right) dY \tag{29d}$$

In a similar way, for the load case of $m = h = 1$, we apply a unit initial strain in the y_1 direction, as given in Equation (30). Then, the overall properties listed in Equation (31) can found.

$$\boldsymbol{\varepsilon}_0^{11} = [\,1 \quad 0 \quad 0 \quad 0 \quad 0 \quad 0 \quad 0 \quad 0 \quad 0\,]^T \tag{30}$$

$$\bar{C}_{11} = \frac{1}{V}\int_Y \left(C_{11} + C_{11}\frac{\partial \chi_1^{11}}{\partial y_1} + C_{12}\frac{\partial \chi_2^{11}}{\partial y_2} + C_{13}\frac{\partial \chi_3^{11}}{\partial y_3} + e_{31}\frac{\partial \Gamma^{11}}{\partial y_3} \right) dY \tag{31a}$$

$$\bar{C}_{21} = \frac{1}{V}\int_Y \left(C_{21} + C_{21}\frac{\partial \chi_1^{11}}{\partial y_1} + C_{22}\frac{\partial \chi_2^{11}}{\partial y_2} + C_{23}\frac{\partial \chi_3^{11}}{\partial y_3} + e_{32}\frac{\partial \Gamma^{11}}{\partial y_3} \right) dY \tag{31b}$$

$$\bar{C}_{31} = \frac{1}{V}\int_Y \left(C_{31} + C_{31}\frac{\partial \chi_1^{11}}{\partial y_1} + C_{32}\frac{\partial \chi_2^{11}}{\partial y_2} + C_{33}\frac{\partial \chi_3^{11}}{\partial y_3} + e_{33}\frac{\partial \Gamma^{11}}{\partial y_3} \right) dY \tag{31c}$$

$$\bar{e}_{31} = \frac{1}{V}\int_Y \left(e_{31} + e_{31}\frac{\partial \chi_1^{11}}{\partial y_1} + e_{32}\frac{\partial \chi_2^{11}}{\partial y_2} + e_{33}\frac{\partial \chi_3^{11}}{\partial y_3} - k_{33}\frac{\partial \Gamma^{11}}{\partial y_3} \right) dY \tag{31d}$$

It is a common practice to apply periodic boundary conditions on the RVE to find the homogenized coefficients. Therefore, the local displacements and electric potential should be specified on the opposite boundary surface of the RVE. For example, for the corresponding node i and j on the opposite surface of RVE, they should be prescribed as

$$\chi_k^{mh}(i) = \chi_k^{mh}(j), \Gamma^{mh}(i) = \Gamma^{mh}(j) \quad (k = 1, 2, 3) \tag{32}$$

To realize the boundary conditions in Equations (32), one of the common measure is to introduce penalty function in the final assembly stiffness matrix. However, this will be very time-consuming in numerical calculation. A simple treatment is to adopt 1/8 of the RVE, where the normal mechanical displacements are constrained on the six surfaces of the hexagonal RVE,[21] that is,

$$\chi_1^{mh} = 0, \sigma_{21} = \sigma_{31} = 0, \text{when } y_1 = 0 \text{ and } y_1 = a/2 \tag{33a}$$

$$\chi_2^{mh} = 0, \sigma_{12} = \sigma_{32} = 0, \text{when } y_2 = 0 \text{ and } y_2 = a/2 \tag{33b}$$

$$\chi_3^{mh} = 0, \sigma_{13} = \sigma_{23} = 0 \text{ when } y_3 = 0 \text{ and } y_3 = h/2 \tag{33c}$$

As to the electrical boundary conditions, vanishing electric potentials are given on the upper and bottom surfaces,[21] while on the four side-surfaces of the hexagonal RVE, the electric displacement is prescribed to be continuous along the normal direction.

The local analysis was carried out on 1/8 of the RVE in ANSYS under the loads in Equations (28) and (30), respectively, from which the electromechanical fields on the microscopic level can be solved. The overall properties, that is, $\bar{C}_{13} = \bar{C}_{23}$, $\bar{C}_{33}$, $\bar{e}_{33}$, $\bar{C}_{11}$, and $\bar{e}_{31}$, can be obtained in terms of the Equations (29) or (31). It should be noted that, in the estimation of the integrals in Equations (29a)–(29d) or (31a)–(31d), numerical methods should be used. Here, we adopt the Gauss integral using $2 \times 2 \times 2$ Gauss points.

3. Results and discussion

3.1. Dependence of the effective properties on various parameters

Since cellular piezoelectret film usually exhibits remarkable quasi-piezoelectric effect in the thickness direction and negligibly small effect in other directions, we here only consider the piezoelectric stress coefficient in the thickness direction, that is, $e_{33} = q(1 + k + k^2)/(1 + k)$, Where k is the aspect ratio of microvoids given by Equation (18). Other coefficients are vanishingly small and ignored.[14] The host polymer is chosen as PP, with the Young's modulus $Y = 1.4$ GPa, Poisson's ratio $v = 0.34$ and the relative dielectric permittivity $\varepsilon_r = 2.2$. In the analysis by AHM plus FEM, the constituents in the periodic composite should be taken as solid phases with certain elastic moduli. However, the inclusions in cellular piezoelectret film are actually the charged voids with a vanishing modulus. To carry out the analysis in finite element program, general practice is to assign a very small modulus rather than zero modulus. For example, here in this simulation, we choose the Young's modulus $Y_{\text{void}} = 1.4 \times 10^{-6}$ GPa, which is six orders of magnitude smaller than the modulus of polymer matrix. Though this value is arbitrarily given, the variation of the effective properties using different Y_{void} is usually negligibly small as long as Y_{void} is kept to be several orders of magnitude smaller than the polymer matrix. The Poisson's ratio of voids is $v = 0$ and the relative dielectric permittivity is $\varepsilon_r = 1$. The electric charge density inside microvoids is generally chosen $q = 0.35 \times 10^{-3} C/m^2$.[14] In the simulation, the geometric model of the hollow oblate tetrakaidecahedron should be pre-established in terms of the void aspect ratio, k, given in Equation (18) and the void fraction, f, in Equation (19), where the wall thickness is kept to be unit, that is, $t = 1$.

In this section, we show the dependence of the effective electromechanical properties on various parameters. In Figures 4 and 5, the electromechanical properties are shown with

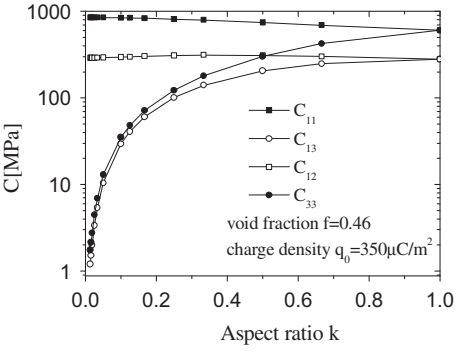

Figure 4. The effective elastic moduli vs. the void aspect ratio.

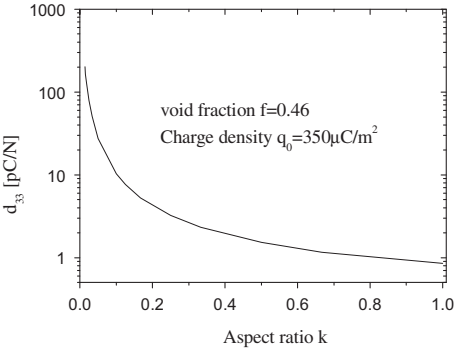

Figure 5. The effective piezoelectric coefficient, d_{33}, vs. the void aspect ratio

respect to the aspect ratio of voids. The overall elastic moduli, including in-plane moduli, C_{11} and C_{12}, and out-of-plane elastic moduli, C_{13} and C_{33}, are demonstrated with respect to the void aspect ratio (Figure 4). The in-plane moduli generally decrease and the out-of-plane moduli increase as the aspect ratio increases. This coincides with experiments revealing that as microvoids turn to round shape, the piezoelectret film becomes stiffer in the film thickness direction. When the aspect ratio equals to unit one, that is, $k = 1$, then the shape anisotropy disappears. The in-plane tensile modulus, C_{11}, is identical to the out-of-plane modulus, C_{33}, while the in-plane shear modulus, C_{12}, equals to the out-of-plane shear modulus, C_{13}. The elastic behavior of cellular piezoelectret film becomes isotropic. From Figure 5, it can be seen that piezoelectric coefficient d_{33} decreases as aspect ratio increases. This is in agreement to the general experimental results as well as theoretical predictions that d_{33} varies oppositely to the C_{33} as the aspect ratio changes.[11–14]

Figures 6 and 7 show the overall elastic moduli and piezoelectric coefficients vs. the void volume fraction. In Figure 6, it can be seen that the elastic moduli decrease as void volume fraction increases. This is because cellular piezoelectret film becomes more and more flexible and the effective elastic moduli decrease as the void volume fraction increases. In Figure 7, the piezoelectric coefficients in the film thickness direction d_{33} and also the transverse direction, $d_{31} = d_{32}$, are plotted against the void volume fraction. Opposite to elastic moduli, the piezoelectric coefficients increase as the void volume fraction increases. This also coincides to the general experimental findings and theoretical predictions that the effective piezoelectric coefficients vary inversely with the elastic moduli.[11–14]

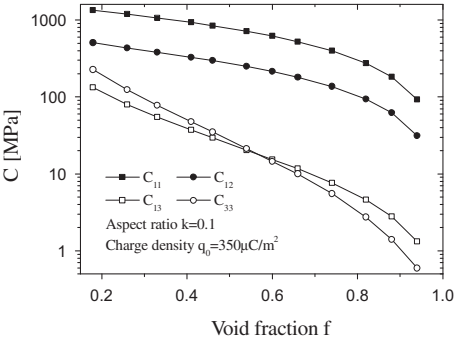

Figure 6. The effective elastic moduli vs. the void volume fraction.

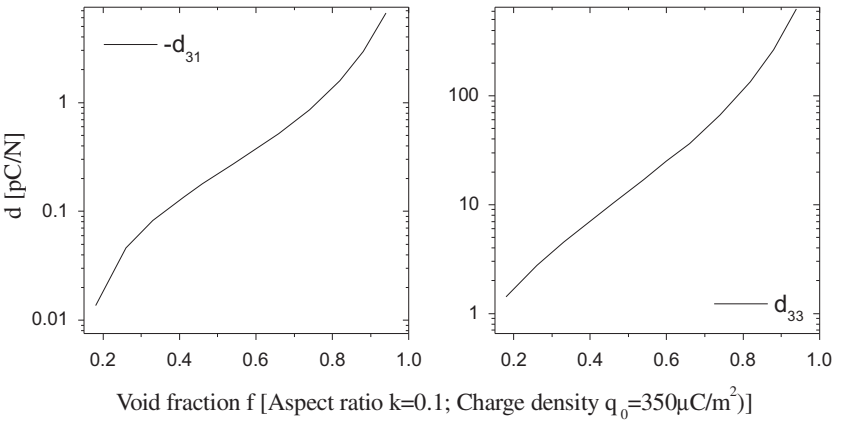

Figure 7. The effective piezoelectric coefficients vs. the void volume fraction.

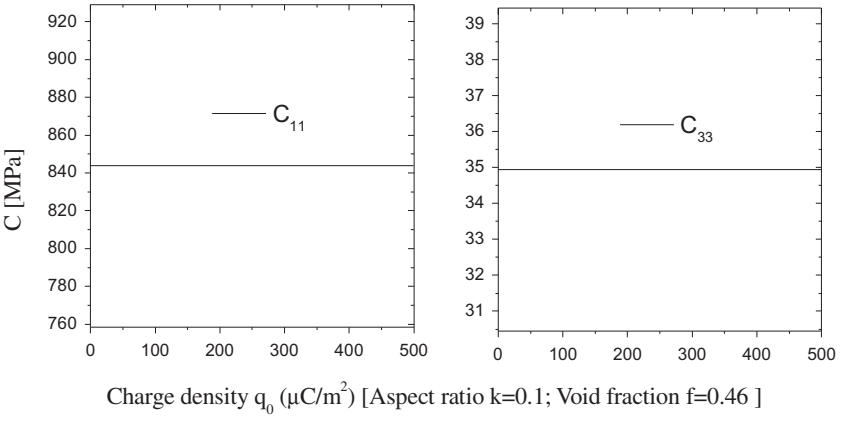

Figure 8. The effective elastic moduli vs. the charge density of voids.

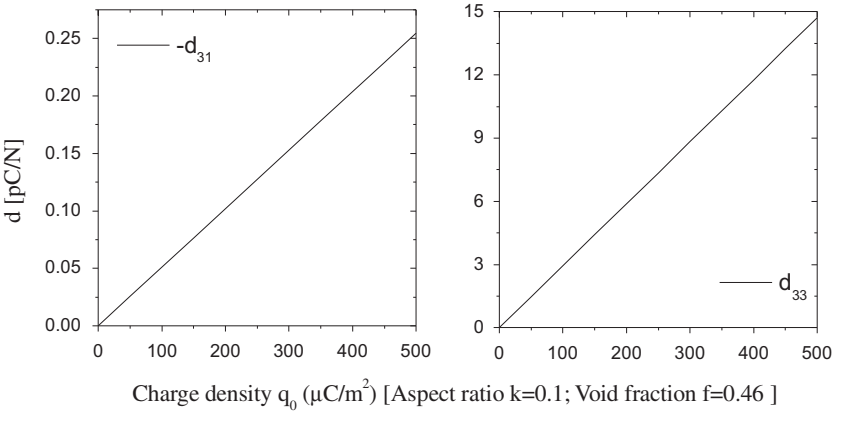

Figure 9. The effective piezoelectric coefficients vs. the charge density of voids.

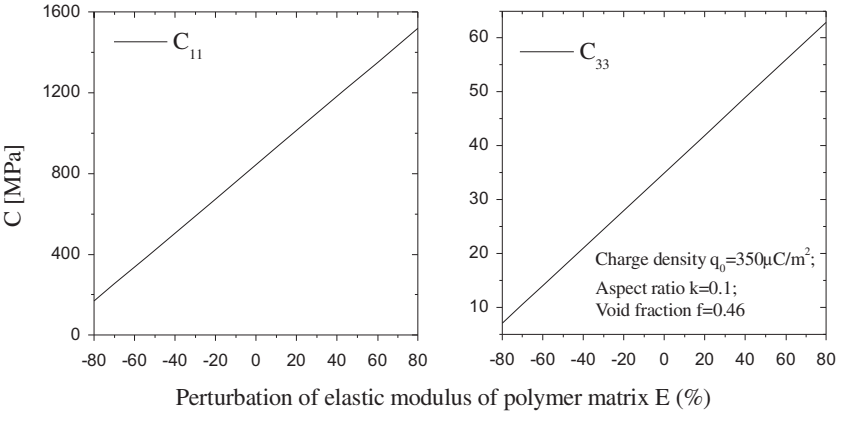

Figure 10. The effective elastic moduli vs. the perturbation of Young's modulus of matrix.

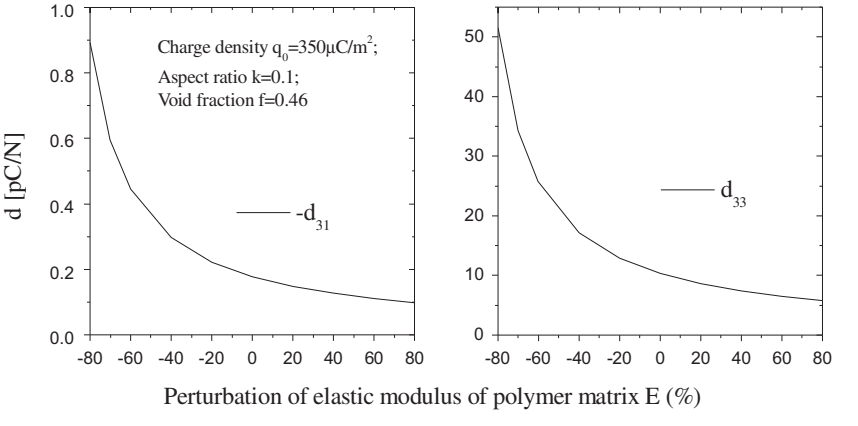

Figure 11. The effective piezoelectric coefficients vs. the perturbation of Young's modulus of matrix.

In addition, we also investigate the effect of the electric charge density inside microvoids on overall elastic moduli and piezoelectric coefficients. Figure 8 shows the overall elastic moduli vs. the charge density of voids. No obvious effect can be detected to the elastic moduli when the charge density varies. However, as indicated in Figure 9, the piezoelectric coefficients, both d_{33} and $d_{31}(d_{32})$, almost increase linearly with respect to the charge density. Figures 10 and 11 present the dependence of the overall electromechanical properties on the Young's modulus of polymer matrix. In Figures 10 and 11, a perturbation is assumed to the Young's modulus of the polymer matrix and the overall elastic moduli and piezoelectric coefficients were calculated. It is shown that the overall elastic moduli, both C_{11} and C_{33}, increase with the Young's modulus of matrix while the piezoelectric coefficients, that is, d_{33} and d_{31} indicated in Figure 11, decrease.

3.2. Simulation of experimental results

Experiments in the literature [6] confirmed that, by adjusting the microvoid structure through controlled inflation, cellular piezoelectret film can reach the maximum piezoelectric

coefficients. It was pointed out [13,14,18] that both the void aspect ratio and the void volume fraction change in the inflation process, which can be correlated by

$$f + \rho/\rho_{PP} = 1 \tag{34}$$

where ρ and ρ_{PP} are, respectively, the density of cellular piezoelectret film and the density of polymer matrix, ρ/ρ_{PP} is the relative density. To simulate the experimental results of the overall C_{33} and d_{33} at different densities,[6] similar to the previous theoretical analyses, a certain relation should be given between the void volume fraction and the void aspect ratio. Though this relation should be basically quantified by experiments, the cubic polynomial function is usually used.[13,14,18] A similar relation was also adopted in this simulation as follows:

$$k = 0.0866f^3 + 0.1577f^2 - 0.1747f + 0.0493 \tag{35}$$

in which k and f are given in Equations (18) and (19), respectively. Other material parameters and geometric variables are given in subsection 3.1. The simulated results are shown in Figures 12 and 13. It can be seen that the numerical analysis based on AHM plus FEM is also capable of simulating the experimental results of cellular piezoelectret films.

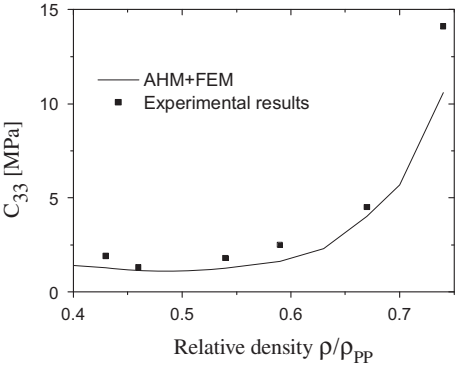

Figure 12. The elastic modulus, C_{33}, vs. the relative density of cellular piezoelectret film.

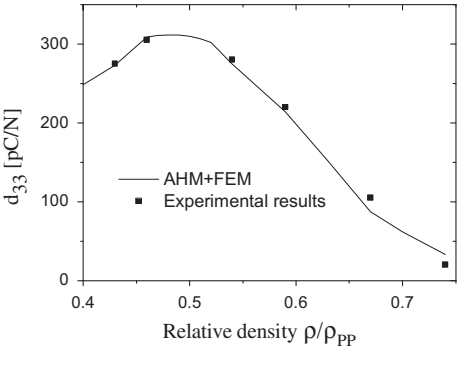

Figure 13. The piezoelectric coefficient, d_{33}, vs. the relative density of cellular piezoelectret film.

4. Conclusions

As a member of the flexible electromechanical materials, cellular piezoelectret film has recently gained much attention in the field of compliant transducer and sensor. The quasi-piezoelectric effect depends strongly on the microstructures of voids scattered in film. Optimum design of this voided charged polymer film is highly demanded. Numerical analysis method should be developed. Since there usually exist a large amount of microvoids, the analysis directly based on finite element on a microscale level usually leads to huge amount of calculation work. In this study, by taking the cellular piezoelectret film as the piezoelectric composite where the charged flat voids are considered as piezoelectric inclusions scattered periodically in the host polymer matrix, we simulate the overall properties by using the asymptotic homogenization implemented by FEM on the RVE. The effective electromechanical properties of cellular piezoelectret film can be numerically obtained. Dependence of the overall electromechanical properties on various material parameters and geometric variables of microvoids has been explored. Furthermore, the results of inflation experiment of cellular piezoelectret film in the literature were also numerically simulated. Both the qualitative analysis and quantitative comparison suggest that the asymptotic homogenization based on finite element analysis is capable of simulating the overall properties of cellular piezoelectret film. This approach is expected to be an efficient mean for the numerical analysis of the overall properties in the optimization design of cellular piezoelectret film with complex microvoid structures.

Acknowledgments

This study was supported by National Natural Science Foundation of China (Project Nos. 11072179, 11090334). Partial support from the Fundamental Research Funds for the Central Universities is also acknowledged.

References

[1] Hillenbrand J, Sessler GM. Piezoelectricity in cellular electret films. IEEE Trans. Dielect. Elect. Insul. 2000;7:537–542.
[2] Lindner M, Hoislbauer H, Schwodiauer R, Bauer-Gogonea S, Bauer S. Charged cellular polymers with ferroelectretic behavior. IEEE Trans. Dielect. Elect. Insul. 2004;11:255–263.
[3] Bauer S, Gerhard-Multhaupt R, Sessler GM. Ferroelectrets: soft electroactive foams for transducers. Phys. Today 2004;57:37–43.
[4] Neugschwandtner GS, Schwbdiauer R, Vieytes M, Bauer-Gogonea S, Bauer S, Hillenbrand J, Kressmann R, Sessler GM, Paajanen M, Lekkala J. Large and broadband piezoelectricity in smart polymer-foam space-charge electrets. Appl. Phys. Lett. 2000;77:3827–3829.
[5] Xia Z. Improved charge stability in polymer electrets quenched before charging. IEEE Trans. Electr. Insul. 1990;25:611–615.
[6] Wegener M, Wirges W, Gerhard-Multhaupt R, Dansachmuller M, Schwodiauer R, Bauer-Gogonea MR, Bauer S, Paajanen M, Minkkinen H, Raukola J. Controlled inflation of voids in cellular polymer ferroelectrets: optimizing electromechanical transducer properties. Appl. Phys. Lett. 2004;84:392–394.
[7] Zhang X, Hillenbrand J, Sessler GM. Piezoelectric d33-coefficient of cellular polypropylene subjected to expansion by pressure-treatment. Appl. Phys. Lett. 2004;85:1226–1228.
[8] Huang J, Zhang X, Xia Z, Wang X. Piezoelectrets from laminated sandwiches of porous polytetrafluoroethylene films and nonporous fluoroethylenepropylene films. J. Appl. Phys. 2008;103:084111.
[9] Paajanen M, Välimäki H, Lekkala J. Modelling the electromechanical film (EMFi). J. Electrostat. 2000;48:193–204.
[10] Paajanen M, Lekkala J, Valimaki H. Electromechanical modeling and properties of the electret film EMFi. IEEE Trans. Dielect. Elect. Insul. 2001;8:629–636.

[11] Sessler GM, Hillenbrand J. Electromechanical response of cellular electret films. Appl. Phys. Lett. 1999;75:3405–3407.
[12] Hillenbrand J, Sessler GM, Zhang X. Verification of a model for the piezoelectric d33-coefficient of cellular electret films. J. Appl. Phys. 2005;98:064105.
[13] Haberman MR, Berthelot YH. A differential effective medium model for piezoelectret foams. J. Appl. Phys. 2007;102:124903.
[14] Wan Y, Xie L, Zhong Z. Micromechanical prediction of the effective electromechanical properties of cellular ferroelectrets. J. Appl. Phys. 2010;108:054101.
[15] Wan Y, Xie L, Zhang X, Zhong Z. Time dependence of piezoelectric d33 coefficient of cellular ferroelectret polypropylene film. Appl. Phys. Lett. 2011;98:122902.
[16] Wan Y, Xie L, Lou K, Zhang X, Zhong Z. Experimental and theoretical study on time dependence of the quasi-piezoelectric d33 coefficients of cellular piezoelectret film. J. Mech. Phys. Solids 2012;60:1310–1329.
[17] Tuncer E, Wegener M, Gerhard-Multhaupt R. Modeling electro-mechanical properties of layered electrets: application of the finite-element method. J. Electrostat. 2005;63:21–35.
[18] Wan Y, Fan L. Modeling the piezoelectric d33 coefficient of the cellular piezoelectret film by finite element method. Mod. Phys. Lett. B 2011;25:2343–2351.
[19] Wan Y, Fan L, Zhong Z. Finite element modeling of temporal evolution of the quasi-piezoelectric d33 coefficient of cellular piezoelectret polypropylene film. Comput. Mater. Sci. 2012;55:54–59.
[20] Hollister SJ, Kikuchi N. A comparison of homogenization and standard mechanics analyses for periodic porous composites. Comput. Mech. 1992;10:73–95.
[21] Silva ECN, Fonseca JSO, Kikuchi N. Optimal design of periodic piezocomposites. Comput. Methods Appl. Mech. Eng. 1998;159:49–77.
[22] Feng M, Wu C. A study of three-dimensional four-step braided piezo-ceramic composites by the homogenization method. Composite. Sci. Tech. 2001;61:1889–1898.
[23] Berger H, Gabbert U, Koppe H, Rodriguez-Ramos R. Finite element and asymptotic homogenization methods applied to smart composite materials. Comput. Mech. 2003;33:61–67.